A small-angle neutron scattering study of nonionic surfactant molecules at the water–oil interface: Area per molecule, microemulsion domain size, and rigidity

T. Sottmann, R. Strey, and S.-H. Chen

Citation: The Journal of Chemical Physics **106**, 6483 (1997); doi: 10.1063/1.473638
View online: http://dx.doi.org/10.1063/1.473638
View Table of Contents: http://scitation.aip.org/content/aip/journal/jcp/106/15?ver=pdfcov
Published by the AIP Publishing

A small-angle neutron scattering study of nonionic surfactant molecules at the water–oil interface: Area per molecule, microemulsion domain size, and rigidity

T. Sottmann, R. Strey,[a),b)] and S.-H. Chen[c)]
Max Planck Institut für Biophysikalische Chemie, Postfach 2841, D-37018 Göttingen, Germany

(Received 30 September 1996; accepted 9 January 1997)

The small-angle neutron scattering (SANS) of bicontinuous microemulsions of 19 different water-*n*-alkane-C_iE_j (*n*-alkylpolyglycolether) systems has been measured. All scattering curves exhibit a broad scattering peak which permits determining the characteristic length scale ξ for bicontinuous structures at symmetric water and oil volume fractions, i.e., $\phi=0.5$. Various random models predict $\xi = a\delta\phi(1-\phi)/\phi_c$. We find that ξ is indeed inversely proportional to the surfactant volume fraction ϕ_c. Approximating the effective surfactant chain length δ by $\delta = \nu_c/a_c$, where a_c and ν_c are the area and the volume of the surfactant molecule, the numerical value for a is determined to be $a = 7.16$, which is close to, but significantly different from those used in theoretical models. The head group area a_c at the water–oil interface is obtained from the large q part of the scattering curves. It is found to be independent of i and k, the carbon numbers of the alkyl chain of the surfactant and of the alkane, respectively. However, it depends strongly, and nearly linearly, on the head group size j of the surfactant. Within experimental error it is described by $a_c = 29.3 + 6.20j$ ($Å^2$). © *1997 American Institute of Physics.* [S0021-9606(97)50315-1]

I. INTRODUCTION

Microemulsions are thermodynamically stable, macroscopically homogeneous mixtures of water(a), oil(b), and surfactant(c). Microscopically, the surfactant forms a film separating the two incompatible solvents into two subphases. In various ways the essential features of microemulsions are controlled by the properties of the interfacial film.

First, the *length scale* in microemulsions is set by the area of the internal interface. $S/V = \phi_{c,i}a_c/\nu_c$, the total (specific) area of the internal interface is determined by the area per surfactant molecule a_c. Here $\phi_{c,i}$ and ν_c denote the volume fraction of surfactant ($_c$) at the interface ($_i$) and the volume per surfactant molecule, respectively. As Porod elaborated, the area of a two-phase medium can be determined from the large q part of the scattered intensity of x rays and neutrons.[1] In this paper we measure S/V and thus determine a_c for a large number of nonionic microemulsion systems.

Second, the *structure* of a microemulsion is determined by the local curvature of the interface. A common reference point for these systems is the optimal point,[2,3] where the microemulsion contains equal volumes of water and oil, and the interfacial film has a zero-mean curvature. Here the microstructure of the microemulsion takes the form of a sponge and is *bicontinuous*.[4] In the past two decades the random structure of bicontinuous microemulsions has been proven and its description perfected. Scriven was first to propose the idea of a bicontinuous network of water and oil.[5] Talmon and Prager modeled it by a Voronoi tesselation.[6] Later De Gennes and Taupin simplified the model by a division into cubes.[7] All bicontinuous models predict a length scale

$$\xi = a\,\frac{\phi(1-\phi)}{(S/V)}, \tag{1}$$

set by the total interfacial area. The models differ only in the absolute numerical value of a. [e.g., $a=4$ (Ref. 8), 5.84 (Ref. 6), 6 (Ref. 7)]. A number of groups[9–11] showed that scattering peaks from bicontinuous microemulsions varied with ϕ the oil-in-water-plus-oil volume fraction according to the random surface description [Eq. (1)], although random models do not necessarily predict a peak. Therefore the question is, which numerical value of a is ''exact''? In this paper we present an experimental determination of a.

Teubner and Strey[12] showed which length-scales cause the scattering peaks in microemulsions. Chen and co-workers[13–15] connected the scattering peaks and the random wave description of Cahn[16] and Berk,[17] while Teubner[18] showed how level surfaces are connected with the mean and the Gaussian curvatures. Anderson *et al.*[19] calculated the variation of mean and Gaussian curvatures with ϕ for the Voronoi tesselation. Pieruschka and Marcelja,[20] and Pieruschka and Safran[21] linked the random wave description with bending elastic properties of the surfactant film. Widom[22] and Cates *et al.*[23] used the random model to explain important features of real microemulsion systems.

Knowledge of the molecular areas per surfactant molecules permits addressing interesting questions concerning the nature of interfacial films. In molecular theories of surfactant self-assembly the area per molecule, the extension of the surfactant chain, the interactions of the surfactant with the solvents, in short, the interfacial stress-profile plays a

[a)]Author to whom correspondence should be addressed.
[b)]Permanent address: Institut für Physikalische Chemie, Universität Köln, D-50939 Köln, Germany.
[c)]Permanent address: Department of Nuclear Engineering and Center for Material Science and Engineering, 24-211, Massachusetts Institute of Technology, Cambridge, Massachusetts 02139.

dominant role.[24,25] Early researchers[26,27] investigated the question, how a surfactant shields the unfavorable water–oil contact. Experience tells that the efficiency of a surfactant increases as the surfactant alkyl chain length is increased.[28] The efficiency of a surfactant is judged from the ultralow values of the interfacial tensions and the associated low amounts of required surfactant.[29] However, one question never really solved was: Is the efficiency increase achieved by a better shielding of the bare water–oil interfacial tension? If this was so, then one might expect a variation of the area per molecule with increasing alkyl-chain length of the surfactants.

Here we report a systematic investigation of the scattering from bicontinuous microemulsions in systems of the type water-*n*-alkane(C_kH_{2k+2})-C_iE_j(C_iH_{2i+1}((O(CH_2)$_2$)$_j$OH). We analyze the Porod region to obtain the area per surfactant molecule. We compare the measured length scale with the prediction of the random surface models and determine the prefactor a in Eq. (1). The knowledge of a is used to elucidate the variation of the areas per molecule with i, j, and k.

II. EXPERIMENT

A. Materials

Long chain surfactants, like Pentaoxyethylene glycol mono-*n*-dodecyl ether ($C_{12}E_5$), were purchased from Fluka (Germany) with a quoted purity of >98%. The shorter chain surfactants were obtained from Bachem (Bubendorf, Switzerland). D_2O (>99.75%) and the *n*-alkanes (>99.5%) were obtained from Merck-Schuchardt (Hohenbrunn, Germany). The compounds were used as purchased. We checked the purity of the surfactants by determining the cloud points of the C_iE_j and comparing them to recommended values by Schubert *et al.*[30]

B. Phase behavior

The phase behavior of the ternary systems water-*n*-alkane -C_iE_j has been described in various connections.[31,32] In Fig. 1 we show a schematic representation of a section through the phase prism at equal volumes of water and oil (ϕ=0.5). At low temperature the microemulsion of o/w type coexists with excess oil (denoted by 2). At high temperature the microemulsion of w/o type coexists with excess water (denoted by 2). At intermediate temperatures, between T_l and T_u, the well-known three-phase body occurs.[2] At $T=(T_l+T_u)/2$ the microemulsion phase contains equal volumes of water and oil, and its structure is known to be bicontinuous. The measurements were performed at a composition indicated schematically in Fig. 1 as point Y. The corresponding surfactant volume fraction ϕ_c is chosen slightly higher than that of point X, in order to have a finite temperature interval for experimentation. Point X denotes the composition of the middle phase coexisting with excess water and oil at T. Although the difference $\phi_c-\phi_c$ was always less than 0.01, it was taken into account when calculating the exact length scale $\bar{\xi}$ referring to point X. Furthermore, the monomeric solubility of surfactant in the subphases $\phi_{c,\mathrm{mon}}$ was accounted for.

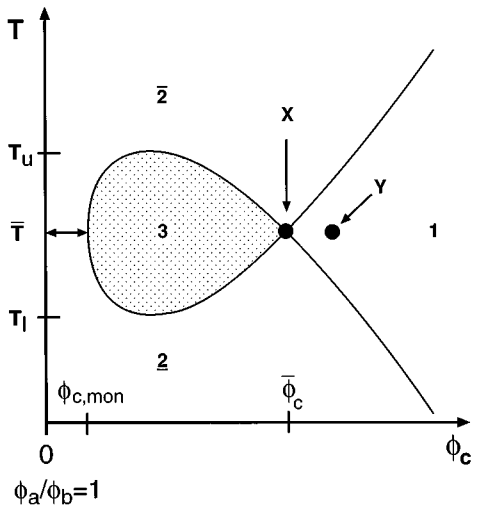

FIG. 1. Vertical section through the phase prism at equal volumes of water and oil (ϕ=0.5) resembling the shape of a ''fish.'' The measurements were performed at point Y.

C. Samples and nomenclature

The sample compositions examined in this paper are given in Table I. Included are the mass fractions (α and γ) and volume fractions (ϕ_i) based on the densities ρ_i (g/cm^3) at 20 °C for D_2O (1.105), *n*-octane (0.702), *n*-decane (0.730), *n*-dodecane (0.751), *n*-tetradecane (0.762), C_6E_2 (0.932), C_8E_3 (0.948), C_8E_4 (0.968), C_8E_5 (0.991), $C_{10}E_4$ (0.959), $C_{10}E_5$ (0.973), $C_{10}E_6$ (0.987), $C_{12}E_4$ (0.950), $C_{12}E_5$ (0.967), and $C_{12}E_6$ (0.980). The temperature dependence of the volume fractions is neglected. The mass fraction α of oil in the mixture of water and oil is denoted by $\alpha=m_b/(m_a+m_b)$, where m_i is the mass component i. The concentration γ of surfactant is calculated from $\gamma=m_c/(m_a+m_b+m_c)$. Also given is the actual temperature of the measurement, close to T. Note that for D_2O the T are about 2 K lower than with H_2O. Also included is the instrument (NG7 or D11) on which the measurement has been performed.

D. Small-angle neutron scattering (SANS) measurements

Small-angle neutron scattering was measured at the National Institute of Standards an Technology (NIST) in Gaithersburg, Maryland, and at the Institute Laue Langevin (ILL) in Grenoble, France.

For the scattering experiments using the NG7 spectrometer at the NIST a mean wavelength of λ_{mean}=5.0 Å having a triangular distribution with full-width at half-maximum (FWHM) of $\Delta\lambda/\lambda$=0.15 was used. The wave vector $q=(4\pi/\lambda)\sin(\Theta/2)$ ranged from 0.004 to 0.55 Å^{-1}, where Θ is the scattering angle. The collimation was fixed at the largest distance to the sample to maximize the resolution. Two sample-

TABLE I. The mass fractions α and γ and the volume fractions ϕ_i of the samples are given along with the measurement temperature and the small angle neutron spectrometer used for the scattering experiment.

i	j	k	System	α	γ	ϕ_a	ϕ_b	ϕ_c	$\phi_{c,i}$	T/ °C	
6	2	8	D_2O-*n*-octane-C_6E_2	0.3887	0.3434	0.3318	0.3318	0.3364	0.3014	4.1	NG7
8	3	8	D_2O-*n*-octane-C_8E_3	0.3885	0.1909	0.4082	0.4082	0.1836	0.1760	13.9	NG7
8	3	10	D_2O-*n*-decane-C_8E_3	0.3979	0.2311	0.3872	0.3877	0.2251	0.2178	20.4	NG7
8	3	12	D_2O-*n*-dodecane-C_8E_3	0.4049	0.2768	0.3638	0.3638	0.2724	0.2653	26.0	NG7
8	3	14	D_2O-*n*-tetradecane-C_8E_3	0.4079	0.3257	0.3390	0.3385	0.3225	0.3155	31.4	NG7
8	4	8	D_2O-*n*-octane-C_8E_4	0.3884	0.2390	0.3866	0.3866	0.2268	0.2197	39.5	NG7
8	5	8	D_2O-*n*-octane-C_8E_5	0.3883	0.2809	0.3686	0.3686	0.2628	0.2561	58.7	NG7
10	4	8	D_2O-*n*-octane-$C_{10}E_4$	0.3886	0.1043	0.4503	0.4508	0.0989	0.0937	22.7	NG7/D11
10	4	10	D_2O-*n*-decane-$C_{10}E_4$	0.3976	0.1349	0.4353	0.4348	0.1299	0.1245	28.3	NG7
10	4	12	D_2O-*n*-dodecane-$C_{10}E_4$	0.4053	0.1696	0.4169	0.4169	0.1652	0.1598	33.5	D11
10	4	14	D_2O-*n*-tetradecane-$C_{10}E_4$	0.4081	0.2093	0.3975	0.3975	0.2050	0.1998	38.3	NG7
10	5	8	D_2O-*n*-octane-$C_{10}E_5$	0.3884	0.1440	0.4325	0.4325	0.1350	0.1301	42.2	NG7
10	6	8	D_2O-*n*-octane-$C_{10}E_6$	0.3886	0.1786	0.4168	0.4173	0.1659	0.1613	58.9	NG7
12	4	8	D_2O-*n*-octane-$C_{12}E_4$	0.3885	0.0300	0.4856	0.4856	0.0288	0.0243	11.0	D11
12	5	8	D_2O-*n*-octane-$C_{12}E_5$	0.3882	0.0562	0.4740	0.4735	0.0525	0.0486	30.6	D11
12	5	10	D_2O-*n*-decane-$C_{12}E_5$	0.3974	0.0728	0.4654	0.4650	0.0696	0.0652	36.2	D11
12	5	12	D_2O-*n*-dodecane-$C_{12}E_5$	0.4046	0.0971	0.4535	0.4530	0.0935	0.0893	41.1	D11
12	5	14	D_2O-*n*-tetradecane-$C_{12}E_5$	0.4081	0.1269	0.4385	0.4385	0.1230	0.1189	46.2	NG7
12	6	8	D_2O-*n*-octane-$C_{12}E_6$	0.3887	0.0792	0.4633	0.4633	0.0734	0.0694	46.8	D11

to-detector distances were measured (10.0 m and 1.3 m) with the detector 25 cm off axis to provide data over a large q-range.

For measurements at the ILL a mean wavelength of $\lambda_{mean}=6.0$ Å with $\Delta\lambda/\lambda=0.10$ was used at the D11 spectrometer. The q ranged from 0.0043 to 0.32 $Å^{-1}$. The collimation was adjusted in order not to limit the resolution. Three sample-to-detector distances were measured (13.0 m, 4.0 m, and 1.1 m) with the detector on axis.

Samples were equilibrated (in half-filled Hellma quartz cells of 1 mm optical pathlength) at the temperature of interest in a separate water bath, and were then rapidly transferred to the cell holder. At the NIST the cell holder was preset to and kept at the desired temperature to within 0.1 °C. After the sample had thermally equilibrated in the cell holder a quick check of homogeneity was performed. Also after the measurement the homogeneity of the sample was checked. At the ILL a homebuilt cell holder, preset to and kept at the desired temperature to within 0.02 °C, allowed the samples to be tilted and thereby mixed and homogenized after mounting. More details have been given previously.[33,34] At the ILL the samples were measured in Hellma quartz cell of 0.2 mm optical path length in order to minimize multiple scattering. Data were collected until the noise level became insignificant.

E. Raw data treatment

The data from the two-dimensional detectors were masked, normalized and radially averaged according to the standard procedures provided by the neutron facilities. Each data set was put on absolute scale by either measuring the scattering of a silica standard provided by the NIST, or by the incoherent scattering of H_2O at the ILL. In previous work we have compared both methods and found good agreement.[34] Data sets from the different distances overlapped without scale adjustment. A few data points of the lowest and highest q values were cut from each set. Pronounced geometrical smearing effects at the lowest q of each sample-to-detector distance were observed at the NIST, with the smearing being stronger for shorter distances. Therefore, the data measured at the longer distance were retained as much as possible in favor of the low q portions measured with the shorter distance. The major smearing of the data are the result of the wavelength spreads, and in the data analysis this effect is taken into account.

III. SCATTERING THEORY

A. The scattering peak

As mentioned in the Introduction the characteristic length scale in microemulsions can be determined from the scattering peak observed by SANS. Following Teubner and Strey[12] one may fit them to

$$I(q)=\frac{8\pi\langle\eta^2\rangle/\xi_{TS}}{p^2-2q_{\max}^2q^2+q^4}+I_{\text{incoh}}, \tag{2}$$

where $p^2=(2\pi/d_{TS})^2+1/\xi_{TS}^2$ and $q_{\max}^2=(2\pi/d_{TS})^2-1/\xi_{TS}^2$. $\langle\eta^2\rangle$ is the mean square scattering length density fluctuation, which for a two phase medium may be approximated by $\langle\eta^2\rangle=\phi_1\phi_2(\Delta\rho)^2$, where $\Delta\rho$ is the difference in scattering length density in the two subphases. I_{incoh} is an incoherent background. Chen *et al.*[35] analyzed the ratio of the correlation length to the periodicity, ξ_{TS}/d_{TS}, and found that it can be interpreted as a measure for the polydispersity of disordered water and oil domains. Experimentally, we will see below that $d_{TS}\approx 2\xi_{TS}$ to a very good approximation. Therefore, we use half the periodicity, $d_{TS}/2$, as the characteristic length scale and define $\xi\equiv d_{TS}/2$. Also, for a symmetric lamellar phase one has exactly $\xi_{TS}=d_{TS}/2$. Loosely one might speak of this length as a mean diameter of a water or

an oil domain. We note that an identification (similar in spirit, although not exactly the same), $\xi=\pi/q_{\max}$, has previously been used.[36]

B. The Porod region and the invariant

Although Eq. (2) has been a useful model description of the peak region in a number of cases, it may not always be exactly correct for the large q part. Two model-independent relations are given by Porod[1]

$$Q=\int_0^\infty q^2 I(q)dq=2\pi^2\langle\eta^2\rangle \tag{3}$$

and

$$\lim_{q\to\infty}[I(q)]=2\pi\langle\Delta\rho^2\rangle\,\frac{S}{V}\,q^{-4} \tag{4}$$

permitting us to extract the total specific internal interface S/V. As can be seen dividing by the ''invariant'' Q [Eq. (3)] the inaccuracy in the absolute calibration of $I(q)$ drops out.[1]

C. Diffuse profiles

As has been noted before the large q portion of the scattering curve may be affected by the diffuseness of the interface.[37,38] For a more precise description one has to include this effect. Assuming the scattering length density profile to change smoothly across the interface Strey *et al.*[37] took this effect into account by convolution of the usual step-profile in the scattering length density with a Gaussian of standard deviation t. In effect it amounts to multiplying the right-hand side of Eq. (4) by $\exp(-q^2t^2)$. By subtracting the incoherent part and using Eqs. (3) and (4) one obtains

$$\frac{S}{V}=\pi\phi_1\phi_2 q^4 e^{q^2t^2}\,\lim_{q\to\infty}[I(q)-I_{\text{incoh}}]/Q. \tag{5}$$

Using Eq. (5) values for S/V are obtained directly from the scattering curves. Note that the exponential term in Eq. (5) for $qt>0.2$ exceeds unity by more than the experimental error and accordingly has to be taken into account.

IV. RESULTS

In Fig. 2 a typical scattering curve for bicontinuous microemulsions is shown for water-*n*-octane-$C_{10}E_4$ measured in a 1 mm cell. As can be seen the scattering peak is well described by Eq. (2). Deviations at about twice $q_{\max}$ might in principle be analyzed in term of a q^{-6} contribution.[39] However, the deviations seem to be dependent, at least in part, on the cell thickness. Repeating the experiment with a 0.2 mm cell the deviations become less pronounced quantitatively, but the peak position is nicely reproduced (cf. Table II). We, therefore, refrain in this paper to analyze the region of about twice $q_{\max}$ of the scattering curve. Concentrating on the peak region we obtain in Table II the fit parameters d_{TS} and ξ_{TS} for the variety of systems investigated. From Table II one can see that $d_{TS}/\xi_{TS}=2.06$, averaged over all 19 systems. If we exclude C_6E_2, because it is the verge of being less well-structured[34] the ratio is 2.02. This finding, we feel, justifies the choice $\xi=d_{TS}/2$.

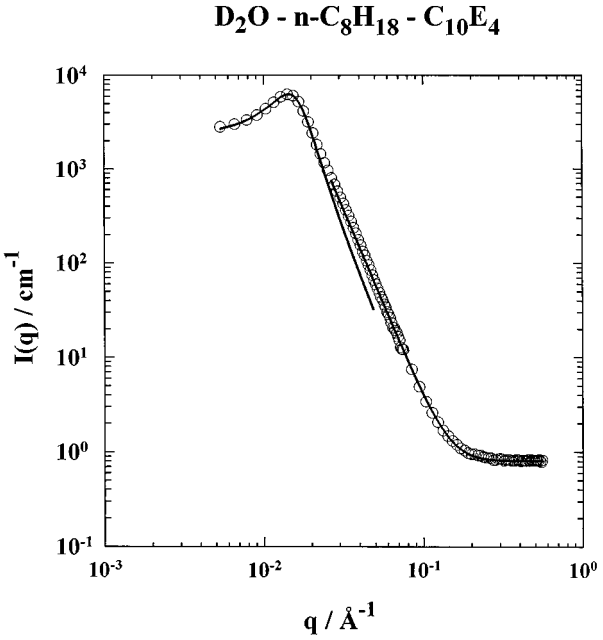

FIG. 2. Typical scattering curve for a bicontinuous microemulsion in the D_2O-*n*-octane-$C_{10}E_4$ system measured in a 1 mm cell. As can be seen the scattering peak is well described by Eq. (2). At large q the scattering curve follows $q^{-4}e^{-q^2t^2}+I_{\text{incoh}}$, which is the Porod decay for diffuse profiles including an experimentally determined incoherent background.

Rearranging Eq. (5) one sees that at large q the intensity should go as $q^{-4}e^{-q^2t^2}+I_{\text{incoh}}$. In Fig. 2 it is shown that the large q part indeed exhibits this dependence, where the incoherent background I_{incoh} has been precisely measured (as opposed to merely calculating it from the incoherent scattering of the components, which is less accurate). As explained above, from fits of the large q part of the curves S/V is obtained. For ϕ_1 and ϕ_2 the protonated and deuterated volume fractions, respectively, were taken using the compositions compiled in Table I. Typically, the q-range chosen for the evaluation was $0.5<qt<0.8$. This choice was a trade-off. On the one hand, one is interested in the local area which means as large q as possible. On the other hand, the coherent part of the intensity should at least be equal or larger than the incoherent background.

A. Determination of the length scale $\bar{\xi}$

Fitting the scattering curves by Eq. (2) one obtains as length scale $\xi\equiv d_{TS}/2$ referring to point Y in Fig. 1. For thermodynamic calculations, interpretation of interfacial tensions, etc. one is interested in the length scale ξ at point X in Fig. 1. This length can be obtained with rather high precision by extrapolation considering that the characteristic length in the system is proportional to the inverse surfactant volume fraction residing at the internal interface. Accordingly, taking into account the monomeric solubility $\underline{\phi}_{c,\text{mon}}=\phi_b\phi_{cmcb}+\phi_a\phi_{cmca}$ in the subphases the length, ξ, corresponding to the fish tail point X, is obtained from

TABLE II. Fit parameters ξ_{TS} and d_{TS} are obtained from Eq. (2). The specific interfacial area S/V is obtained from the fits of the large q part of the scattering curves using Eq. (5), whereas the length scale ξ, corresponding exactly to the interfacial volume fraction of the surfactant $\phi_{c,i}$ at point X in Fig. 1, is obtained from Eq. (6), a_c is obtained by using Eq. (9) with the experimentally determined prefactor $a=7.16$. The bare rigidity κ_0 is obtained from Eq. (11).

i	j	k	ξ_{TS}/Å	d_{TS}/Å	S/V/Å^{-1}	$\overline{\phi}_{c,i}$	$\overline{\xi}$/Å	a_c/Å^2	κ_0/kT
6	2	8	33.0	96.3	0.047 04	0.2797	51.9	41.8	0.44
8	3	8	89.4	195	0.019 25	0.1661	103	48.0	0.57
8	3	10	73.4	159	0.024 24	0.2085	83.2	47.5	0.51
8	3	12	57.3	127	0.030 05	0.2555	66.1	48.7	0.46
8	3	14	47.4	105	0.035 94	0.3049	54.3	49.7	0.42
8	4	8	71.1	159	0.024 47	0.2093	83.5	53.9	0.51
8	5	8	61.4	134	0.029 05	0.2458	69.7	61.3	0.47
10	4	8	198	412	0.009 15	0.0834	231[a]	53.7	0.73
10	4	8	214	423	0.008 27	0.0834	238[b]	52.3	0.74
10	4	10	155	309	0.012 11	0.1144	168	53.9	0.66
10	4	12	126	240	0.014 15	0.1507	127	54.0	0.59
10	4	14	97	191	0.019 60	0.1891	101	54.4	0.54
10	5	8	151	304	0.012 45	0.1199	165	58.5	0.65
10	6	8	123	233	0.015 34	0.1510	124	67.7	0.59
12	4	8	…	…	…	0.0211	(1000)[c]	(53.8)	(1.06)
12	5	8	429	857	0.004 20	0.0378	550	60.0	0.92
12	5	10	348	652	0.005 41	0.0549	387	58.8	0.83
12	5	12	265	474	0.007 40	0.0792	267	59.0	0.74
12	5	14	184	354	0.010 62	0.1090	193	59.4	0.67
12	6	8	331	570	0.006 03	0.0590	335	69.0	0.81

[a]1.0 mm cell.
[b]0.2 mm cell.
[c]Peak outside q-range, estimated.

$$\overline{\xi}=f\xi, \quad \text{with} \quad f=\frac{\phi_c-\phi_b\phi_{cmcb}-\phi_a\phi_{cmca}}{\overline{\phi_c}-\overline{\phi_b}\phi_{cmcb}-\overline{\phi_a}\phi_{cmca}}. \tag{6}$$

In Table II the surfactant volume fraction residing at the internal interface $\phi_{c,i}=\phi_c-\phi_b\phi_{cmcb}-\phi_a\phi_{cmca}$ and the length ξ are given. The extrapolation factor f ranges between $1.03<f<1.28$ and obviously is the ratio of column 6 and 4 in Table II ($f=2\xi/d_{TS}$). ϕ_{cmcb} is the surfactant volume fraction at the cmc in the oil (b), which usually amounts to a few percent. Due to the low solubility of the C_iE_j in water only for C_6E_2 the monomeric solubility in water, ϕ_{cmca}, gave a significant contribution.

In Fig. 3 the variation of $\overline{\xi}$ with alkyl chain i of the surfactant at constant j for $k=8$ is shown. ξ increases linearly with i by about one order of magnitude with a change of four carbon atoms. The reason for this behavior can be seen in the increased rigidity of the interfacial layers which increases the persistence length.[7] For the different $j=4$, 5 or 6 similar trends are seen.

In Fig. 4 the variation of $\overline{\xi}$ at constant $k=8$ with the surfactant head group size j is shown for $i=8$, 10, and 12. As can be seen ξ decreases somewhat with j. This result is remarkable insofar as the overall size of the surfactant molecule, and along with it the thickness of the interfacial layer, is increasing.

In order to demonstrate the variation of $\overline{\xi}$ for the same surfactant with the alkyl chain of the oil k in Fig. 5, C_8E_3, $C_{10}E_4$, and $C_{12}E_5$ are chosen increasing the surfactant size in an approximately balanced fashion. ξ decreases somewhat with k. Notably, both in Figs. 4 and 5 the observed decrease in $\overline{\xi}$ is accompanied by an increase in $\overline{T}$ (consistent with the overall phase behavior[40]).

The enormous variations of $\overline{\xi}$ are to a large extent a consequence of the variation of the internal interface. This can be demonstrated by plotting in Fig. 6 the length scale ξ vs $\overline{(S/V)}^{-1}=f(S/V)^{-1}$ using the experimentally determined

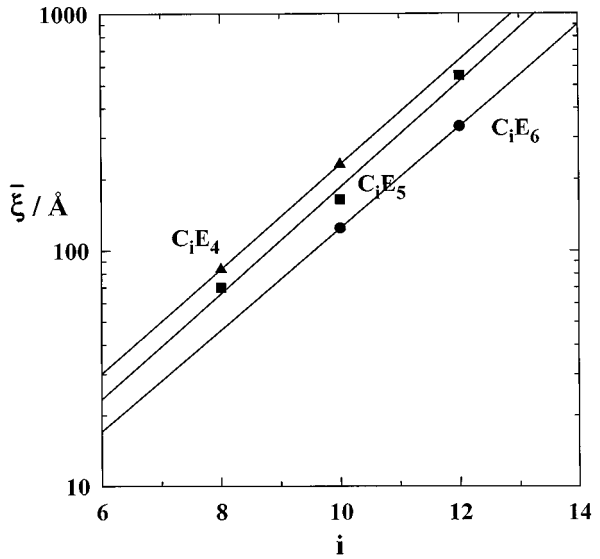

FIG. 3. Variation of the length scale $\overline{\xi}$ (corresponding exactly to the microemulsion at point X in Fig. 1) as function of the carbon number of the alkyl chain of the surfactant i at constant headgroup size j and oil chain length $k=8$.

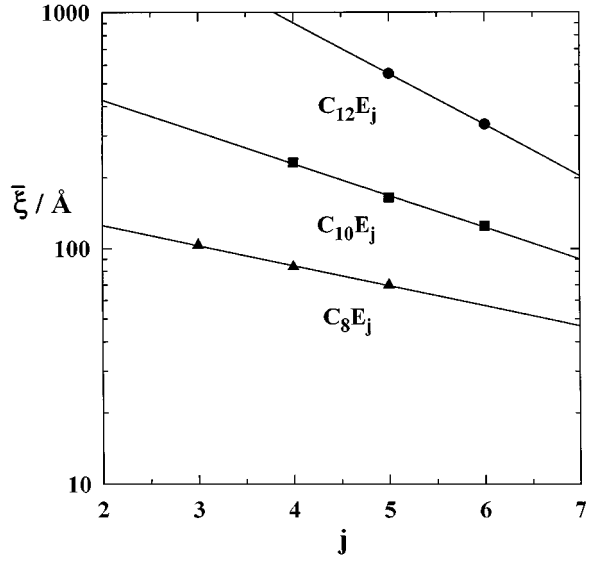

FIG. 4. Variation of the length scale $\bar{\xi}$ at constant $k=8$ as function of the surfactant headgroup size j for $i=8$, 10, and 12.

S/V from Table II, and Eq. (1) valid for the bicontinuous microemulsions at T,

$$\bar{\xi}=a\,\frac{\phi(1-\phi)}{\overline{S/V}}. \tag{7}$$

All data fall on a straight line passing through the origin. Fitting Eq. (7) to the data points,

$$a=7.16 \tag{8}$$

is found. This result constitutes an experimental determination of the prefactor a in Eq. (1) averaged for a whole class of ternary microemulsions. The error bars are calculated by Gaussian error progression. The error in $\bar{\xi}$ comprises errors in the surfactant volume fractions ϕ_c and ϕ_c, the monomeric solubility $\phi_{c,\mathrm{mon}}$ and fitting inaccuracies determining d_{TS}. The combined error in the quantity on the right-hand side of Eq. (7) results from the error in S/V stemming from the Porod analysis [cf. Eq. (5)] and the extrapolation.

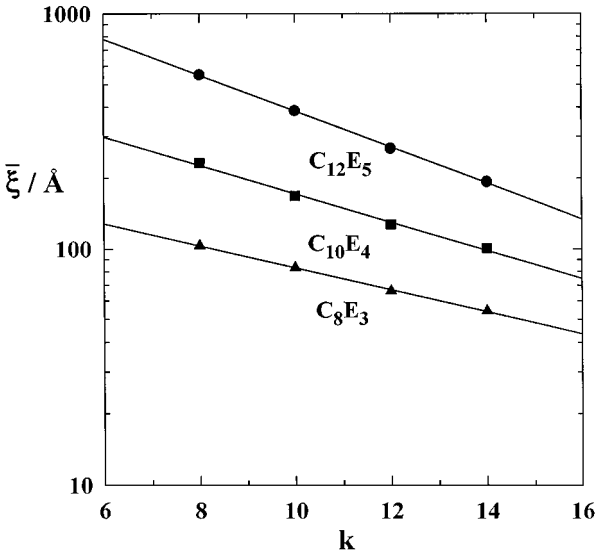

FIG. 5. Variation of the length scale $\bar{\xi}$ at constant i and j as function of the oil chain length k for the C_8E_3, $C_{10}E_4$, and $C_{12}E_5$ systems.

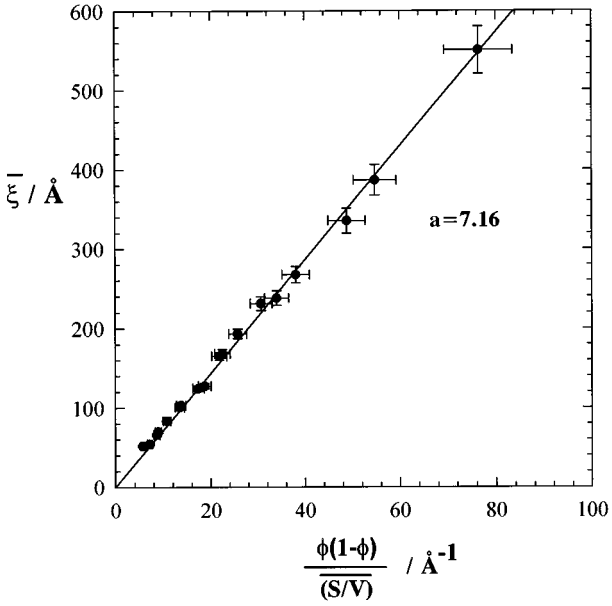

FIG. 6. The length scale $\bar{\xi}$ is plotted vs the right-hand side of Eq. (7) in order to determine the prefactor a using S/V obtained from the large q part of the scattering curves. Note that the data fall on a straight line through the origin with slope $a=7.16$.

B. Determination of the area per molecule a_c

The graph in Fig. 6 has been constructed using the experimentally determined values for S/V subject to the relatively large errors in the large q part of individual scattering curves. Differently, the position of the peak and from it the ξ are more precisely known, as can be seen from the smaller vertical error bars in Fig. 6. The mutual support of the data points in conjunction with Eq. (7) suggests to turn the argument around to obtain rather precise values for a_c from

$$a_c=a\,\frac{\phi(1-\phi)}{\bar{\xi}}\,\frac{\nu_c}{\phi_{c,i}}, \tag{9}$$

where all quantities on the right-hand side are known.

In Fig. 7 a_c determined this way is plotted vs the alkyl chain i of the surfactant together with the error calculated by error progression. Within experimental error no dependence of a_c on the alkyl chain length i of the surfactant is seen. This is remarkable insofar as the interfacial tension[41] between the water and oil excess phase varies over two orders of magnitude as i is increased from 8 to 12.

In Fig. 8 a_c is plotted vs the alkyl chain k of the oil for $C_{12}E_5$, $C_{10}E_4$, and C_8E_3 (top to bottom). No significant dependence of a_c on the alkyl chain length of the oil is seen. It is interesting to note that for the water-*n*-octane-$C_{12}E_5$ system Strey *et al.*[42] recently reported 58.3 Å^2 obtained from a geometric analysis of spherical, cylindrical, and lamellar

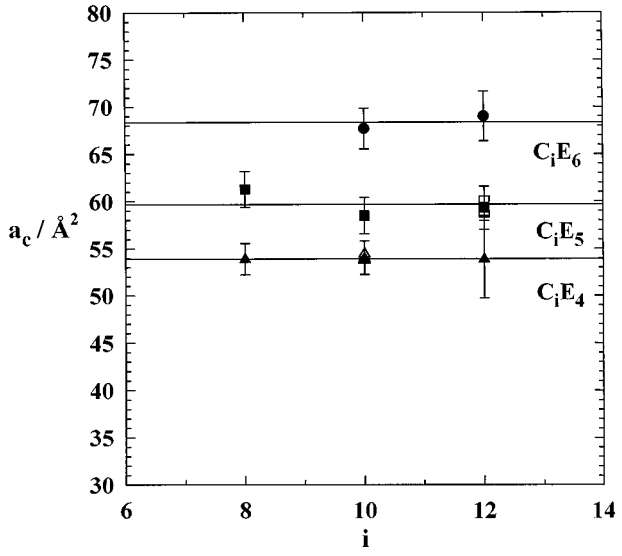

FIG. 7. The area per surfactant molecule a_c is plotted vs the alkyl chain length i of the surfactant at constant oil chain length $k=8$ for $j=4$, 5, and 6. Note that within experimental error a_c is independent of i.

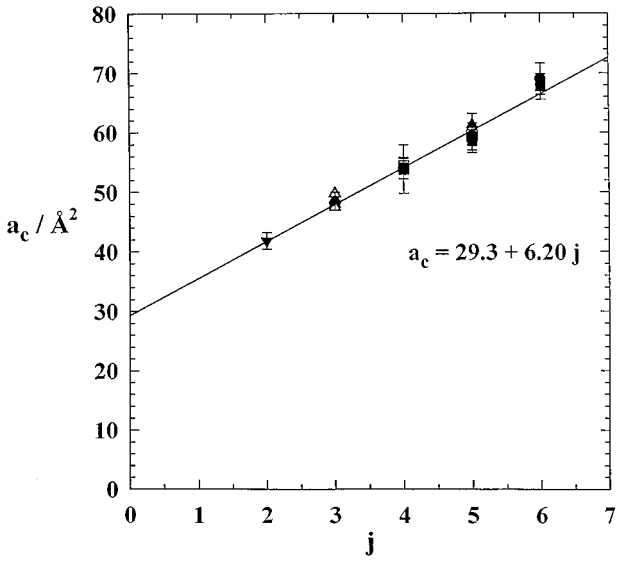

FIG. 9. Variation of the area per surfactant molecule a_c as function of the surfactant headgroup size j for all surfactants and oils. Note that a_c increases linearly with increasing j within experimental error.

structures. The agreement with a_c obtained in this paper from the analysis of large q scattering intensities is remarkable (cf. Fig. 8 and Table II).

In Fig. 9 a_c is plotted vs the head group size j for all surfactants and oils. This is possible because of the observed nondependence on neither the alkyl chain of the surfactant nor the oil. Within experimental error all individual points fall nearly on a straight line. Accordingly, the area per surfactant molecule of the C_iE_j type may rather precisely be calculated from the regression

$$a_c = 29.3 + 6.20j \quad (\text{Å}^2). \tag{10}$$

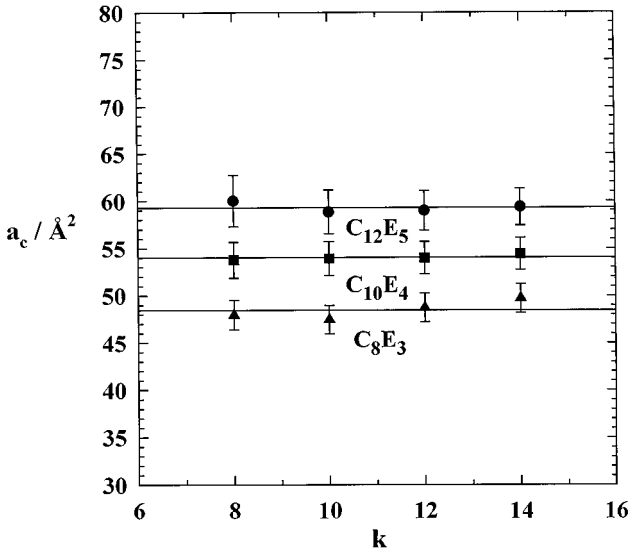

FIG. 8. Variation of the area per surfactant molecule a_c at constant i and j as function of the oil chain length k for C_8E_3, $C_{10}E_4$, and $C_{12}E_5$. Note that within experimental error a_c is independent of k.

C. Determination of κ_0

The length, over which the interfacial film is locally flat, is called the persistence length in analogy with the persistence length in polymers. First introduced by de Gennes and Taupin[7] and later modified by Peliti and Leibler,[43] the expression for the persistence length reads

$$\frac{\xi_\kappa}{\delta} = \exp\left(\frac{4\pi\kappa_0}{3kT}\right), \tag{11}$$

with $\delta = \nu_c/a_c$ being the effective length of the surfactant molecule in the interface. It has previously been suggested to identify the thermodynamically self-adjusting length scale in bicontinuous microemulsions (our ξ) with the persistence length ξ_κ. The argument was that water and oil uptake proceeds until film becomes thermally crumpled.[7] From then on water and oil are expelled as excess phase. This begins to happen exactly at point X to which ξ refers. The experiments performed allow calculating from the persistence length the bare rigidity κ_0 of the film, because all quantities appearing in Eq. (11) are known. The rigidities obtained are given in Table II and are shown in Fig. 10. It is interesting to note that the rigidities are of the order of kT as one might expect. Inspection of Table II, furthermore reveals, that they increase systematically with the alkyl chain length of the surfactant and decrease with the oil chain length.

V. DISCUSSION

The experiments presented allow us to determine more exactly the prefactor a in the expression for the length scale of random bicontinuous structures [Eq. (1)]. The numerical value for a has its roots in the exact topological arrangement of the interfaces in bicontinuous microemulsions. Zemb *et al.* have pointed out that random models do not predict a peak.[44] While this is correct, it does not necessarily mean

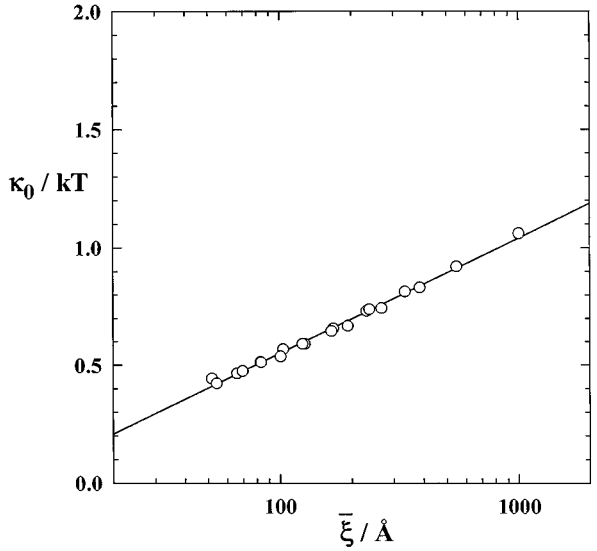

FIG. 10. Bare rigidity κ_0 calculated from the persistence length. Note that, as the surfactant becomes more efficient, the rigidity increases and as a consequence the length scale increases.

that Eq. (1) is not an applicable description of random, or better, disordered bicontinuous microemulsions. On the contrary, as Fig. 6 demonstrates only the numerical prefactor a is different. In this connection one might recall that for the related minimal surfaces in cubic mesophases there are significant differences in the S/V depending on the connectivity or genus of the surfaces. Since the numerical value of a is larger than that for random models, it appears that the higher order as evidenced by the peaks, leads to a ''waste'' of interfacial area.

As mentioned in the Introduction, the length scale in microemulsions is set by the area of the internal interface. If the type of structure is known the system is essentially characterized and varies systematically with the chain lengths of oil and surfactant. The measurements described above permit calculating the length scale from the composition of the mixtures, because the area per surfactant molecule and the prefactor a is now known.

Furthermore, the actual trends of the areas per surfactant molecule with oil chain length, surfactant tail length and head group size are noteworthy.

It is interesting to note that the areas per surfactant molecule at the air–water interface determined by surface tension and neutron reflectivity measurements[45,46] are somewhat (but systematically) lower than the areas determined in this work. There may be various reasons for this fact. One reason is that the liquid–air surface refers to a flat, that is, projected area, while the Porod analysis traces out the actual, possibly undulating surfactant interface. Also, at the air–water interface the film pressure of the alkanes is absent.

VI. CONCLUSIONS

Measuring the scattering peak in bicontinuous microemulsions, as well as the large q part of the scattering curve, we were able to quantify the length scale and the total internal interface. This combined knowledge permitted determining accurate numbers for the interfacial area per surfactant molecule for a whole class of bicontinuous microemulsions. A simple linear dependence on the headgroup size is observed. Furthermore, the prefactor a of the well-known relation $\xi = a(\nu_c/a_c)[\phi(1-\phi)]/\phi_c$ for the length scale in bicontinuous microemulsions could be quantified. Identifying the measured length scale with the persistence length the bare rigidities for 19 different systems is obtained.

ACKNOWLEDGMENTS

We wish to thank Professor M. Kahlweit for support. We also thank our local contacts at the NIST J. Barker and C. Glinka for expert help. Part of the material is based upon activities by the National Science Foundation under Agreement No. DMR-9122444. We acknowledge the support of the Institute of Standards and Technology, U.S. Department of Commerce, in providing the facilities used for some of the experiments. We, furthermore, thank our local contact B. Farago at the ILL.

[1] G. Porod, in *Small Angle X-ray Scattering*, edited by O. Glatter and O. Kratky (Academic, New York, 1982).
[2] M. Kahlweit and R. Strey, Angew. Chem. **97**, 655 (1985).
[3] H. T. Davis, Colloids Surf **A91**, 9 (1994).
[4] B. Lindman, K. Shinoda, U. Olsson, D. Anderson, G. Karlström, and H. Wennerström, Colloids Surf. **38**, 205 (1989).
[5] L. E. Scriven, Nature **263**, 123 (1976).
[6] Y. Talmon and S. Prager, J. Chem. Phys. **69**, 2984 (1978).
[7] P. G. De Gennes and C. Taupin, J. Phys. Chem. **86**, 2294 (1982).
[8] P. Debye, H. R. Anderson, and H. Brumberger, J. Appl. Phys. **28**, 679 (1957).
[9] L. Auvray, J. P. Cotton, R. Ober, and C. Taupin J. Phys. Chem. **79**, 4586 (1984).
[10] J. F. Billman and E. W. Kaler, Langmuir **6**, 611 (1990).
[11] F. Lichterfeld, T. Schmeling, and R. Strey, J. Phys. Chem. **90**, 5762 (1986).
[12] M. Teubner and R. Strey, J. Chem. Phys. **87**, 3195 (1987).
[13] S.-H. Chen, S.-L. Chang, and R. Strey, J. Appl. Crystallogr. **24**, 721 (1991).
[14] S.-H. Chen, D. Lee, and S.-L. Chang, J. Mol. Struct. **296**, 259 (1993).
[15] S.-H. Chen and S.-L. Chang, in *Structure and Dynamics of Strongly Interacting Colloids and Supramolecular Aggregates in Solution*, edited by S. H. Chen *et al.* (Kluwer, Dordrecht, 1992), p. 659.
[16] J. W. Cahn, J. Chem. Phys. **42**, 93 (1965).
[17] N. F. Berk, Phys. Rev. Lett. **58**, 2718 (1987).
[18] M. Teubner, Europhys. Lett. **14**, 403 (1991).
[19] D. M. Anderson, H. T. Davis, and L. E. Scriven, J. Chem. Phys. **91**, 3246 (1989).
[20] P. Pieruschka and S. Marcelja, J. Phys. II **2**, 235 (1992).
[21] P. Pieruschka and S. A. Safran, Europhys. Lett. **31**, 207 (1995).
[22] B. Widom, J. Chem. Phys. **81**, 1030 (1984).
[23] M. E. Cates, D. Andelman, S. A. Safran, and D. Roux, Langmuir, **7**, 2928 (1988).
[24] I. Szleifer, A. Ben-Shaul, and W. M. Gelbart, J. Chem. Phys. **94**, 5081 (1990).
[25] P. A. Barneveld, D. E. Hesselink, F. A. M. Leermakers, J. Lyklema, and J. M. H. M. Scheutjens, Langmuir **10**, 1084 (1994).
[26] L. M. Prince, *Microemulsions* (Academic, New York, 1977).
[27] M. L. Robbins, in *Micellization, Solubilization and Microemulsions*, edited by K. L. Mittal (Plenum, New York, 1976), p. 713.
[28] M. Kahlweit, R. Strey, D. Haase, and P. Firman, Langmuir **4**, 785 (1988).
[29] T. Sottmann and R. Strey, J. Phys. Condensed Matter **8**, A39 (1996).
[30] K.-V. Schubert, R. Strey, and M. Kahlweit, J. Colloid. Interface Sci. **141**, 21 (1991).
[31] M. Kahlweit, R. Strey, and G. Busse, J. Phys. Chem. **94**, 3881 (1990).
[32] M. Kahlweit, R. Strey, and G. Busse, Phys. Rev. E **47**, 4197 (1993).

[33] K.-V. Schubert and R. Strey, J. Chem. Phys. **95**, 8532 (1991).
[34] K.-V. Schubert, R. Strey, S. R. Kline, and E. W. Kaler, J. Chem. Phys. **101**, 5343 (1994).
[35] S.-H. Chen, S.-L. Chang, and R. Strey, Prog. Colloid Polym. Sci. **81**, 30 (1990).
[36] D. Guest, L. Auvray, and D. Langevin, J. Phys. Lett. **46**, L-1055 (1985).
[37] R. Strey, J. Winkler, and L. Magid, J. Phys. Chem. **95**, 7502 (1991).
[38] M. Gradzielski, D. Langevin, L. Magid, and R. Strey, J. Phys. Chem. **99**, 13232 (1995).
[39] S.-H. Chen, D. Lee, and S.-L. Chang, J. Mol. Struct. **296**, 259 (1993).
[40] M. Kahlweit, R. Strey, and P. Firman, J. Phys. Chem. **90**, 671 (1985).
[41] T. Sottmann and R. Strey, J. Chem. Phys. (to be published).
[42] R. Strey, O. Glatter, K.-V. Schubert, and E. W. Kaler, J. Chem. Phys. **105**, 1175 (1996).
[43] L. Peliti and S Leibler, Phys. Rev. Lett. **54**, 1690 (1985).
[44] T. N. Zemb, I. S. Barnes, P.-J. Derian, and B. W. Ninham, Prog. Colloid Polym. Sci. **81**, 20 (1990).
[45] M. J. Rosen, A. W. Cohen, M. Dahanayake, and X. Hua, J. Phys. Chem. **86**, 541 (1982).
[46] J. R. Lu, Z. X. Li, T. J. Su, R. K. Thomas, and J. Penfold, Langmuir **9**, 2408 (1993).